JCI insight

SGLT2 inhibition reprograms systemic metabolism via FGF21-dependent and -independent mechanisms

Soravis Osataphan, … , Robert Gerszten, Mary-Elizabeth Patti

JCI Insight. 2019;4(5):e123130. https://doi.org/10.1172/jci.insight.123130.

Research Article | Hepatology | Metabolism

Graphical abstract

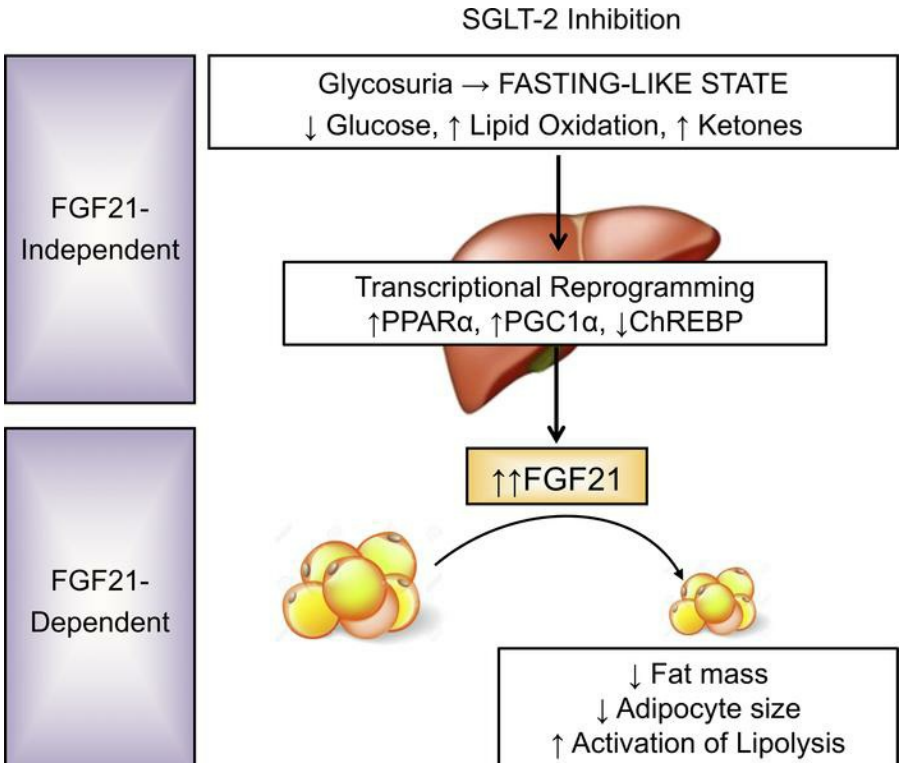

JCI insight

RESEARCH ARTICLE

SGLT2 inhibition reprograms systemic metabolism via FGF21-dependent and -independent mechanisms

Soravis Osataphan,[1,2,3] Chiara Macchi,[1,4] Garima Singhal,[2,5] Jeremy Chimene-Weiss,[1] Vicencia Sales,[1,2] Chisayo Kozuka,[1,2] Jonathan M. Dreyfuss,[2,6] Hui Pan,[2,6] Yanin Tangcharoenpaisan,[1] Jordan Morningstar,[7] Robert Gerszten,[2,7] and Mary-Elizabeth Patti[1,2]

[1]Section of Integrative Physiology and Metabolism, Research Division, Joslin Diabetes Center, Boston, Massachusetts, USA. [2]Harvard Medical School, Boston, Massachusetts, USA. [3]Department of Pathology, Srinakharinwirot University, Bangkok, Thailand. [4]Department of Pharmacological and Biomolecular Sciences, Università degli Studi di Milano, Milan, Italy. [5]Division of Endocrinology and Metabolism, Department of Medicine, Beth Israel Deaconess Medical Center, Boston, Massachusetts, USA. [6]Bioinformatics and Biostatistics Core, Research Division, Joslin Diabetes Center, Boston, Massachusetts, USA. [7]Division of Cardiovascular Medicine, Department of Medicine, Beth Israel Deaconess Medical Center, Boston, Massachusetts, USA.

Pharmacologic inhibition of the renal sodium/glucose cotransporter-2 induces glycosuria and reduces glycemia. Given that SGLT2 inhibitors (SGLT2i) reduce mortality and cardiovascular risk in type 2 diabetes, improved understanding of molecular mechanisms mediating these metabolic effects is required. Treatment of obese but nondiabetic mice with the SGLT2i canagliflozin (CANA) reduces adiposity, improves glucose tolerance despite reduced plasma insulin, increases plasma ketones, and improves plasma lipid profiles. Utilizing an integrated transcriptomic-metabolomics approach, we demonstrate that CANA modulates key nutrient-sensing pathways, with activation of 5′ AMP-activated protein kinase (AMPK) and inhibition of mechanistic target of rapamycin (mTOR), independent of insulin or glucagon sensitivity or signaling. Moreover, CANA induces transcriptional reprogramming to activate catabolic pathways, increase fatty acid oxidation, reduce hepatic steatosis and diacylglycerol content, and increase hepatic and plasma levels of FGF21. Given that these phenotypes mirror the effects of FGF21 to promote lipid oxidation, ketogenesis, and reduction in adiposity, we hypothesized that FGF21 is required for CANA action. Using FGF21-null mice, we demonstrate that FGF21 is not required for SGLT2i-mediated induction of lipid oxidation and ketogenesis but is required for reduction in fat mass and activation of lipolysis. Taken together, these data demonstrate that SGLT2 inhibition triggers a fasting-like transcriptional and metabolic paradigm but requires FGF21 for reduction in adiposity.

Authorship note: SO and CM contributed equally to this work.

Conflict of interest: This work was funded by an investigator-initiated grant from Janssen Pharmaceuticals. MEP received investigator-initiated grant support from Janssen Pharmaceuticals for some of the studies reported in this manuscript. She is a coinvestigator on an NIH R44 grant, together with Xeris Pharmaceuticals; has consulted for Eiger Biopharmaceuticals; has received investigator-initiated grant support from MedImmune, Sanofi, AstraZeneca, Jenesis, and Nuclea; has been a site investigator for XOMA; and acknowledges clinical trial research trial product support from Ethicon, Covidien, NovoNordisk, Nestlé, and Dexcom within the past 5 years.

Submitted: July 10, 2018
Accepted: January 17, 2019
Published: March 7, 2019

Reference information:
JCI Insight. 2019;4(5):e123130.
https://doi.org/10.1172/jci.insight.123130.

Introduction

SGLT2 inhibitors (SGLT2i) are unique antidiabetic drugs that promote urinary glucose loss and increase the urinary threshold for glucose reabsorption. As a result, plasma glucose levels are reduced and overall glycemic control is improved (1, 2). Intriguingly, SGLT2i, including canagliflozin (CANA), have recently been shown to reduce cardiovascular and all-cause mortality in type 2 diabetes (T2D) (3) and may improve hepatic steatosis and nonalcoholic fatty liver disease (4). The cellular actions of SGLT2i are distinct from those of other medications for T2D, such as insulin sensitizers and insulin secretagogues, which reduce blood glucose but increase glucose uptake and promote weight gain. By contrast, SGLT2i act in an insulin-independent manner to cause modest weight loss, promote fatty acid oxidation and ketogenesis, and increase hepatic glucose production (5–7), even after a single dose (8). The unique induction of fatty acid oxidation and ketogenesis by SGLT2i may contribute to not only beneficial outcomes, but also ketoacidosis reported with this medication class (9, 10).

Urinary glucose excretion has been proposed to mediate weight loss effects of SGLT2i but cannot fully account for the observed weight loss (11). In contrast to diet-induced weight loss, there is no reduction in energy expenditure during SGLT2i-induced weight loss (11), potentially as a result of increased lipid oxida-

tion (5). Thus, the precise molecular mechanisms responsible for SGLT2i-mediated effects on metabolism and weight loss remain to be characterized.

Here, we utilize an integrated transcriptomic-metabolomics approach to identify molecular mediators of CANA in nondiabetic mice with diet-induced obesity. We demonstrate that CANA modulates key nutrient-sensing pathways, with activation of 5′ AMP–activated protein kinase (AMPK) and inhibition of mechanistic target of rapamycin (mTOR), without changing insulin or glucagon sensitivity or signaling. Moreover, CANA induces transcriptional reprogramming to activate catabolic pathways, increase fatty acid oxidation, reduce hepatic steatosis, and increase hepatic and plasma levels of the hepatokine FGF21. FGF21 is an important coordinator of fasting-induced metabolic responses and reduction in adiposity via increasing lipolysis, hepatic fatty acid oxidation, and ketogenesis. Given that these effects mirror many phenotypes induced by CANA, we hypothesized that FGF21 would be required for CANA action. Using FGF21-null mice, we demonstrate that FGF21 is not required for the metabolic switch toward a fasting-like catabolic state but is required to promote lipolysis and reduction in adiposity in response to SGLT2i.

Results

CANA reduces blood glucose, improves glucose tolerance, and causes a shift toward lipid utilization. To analyze the metabolic response to SGLT2 inhibition, and to dissect the effect of weight loss in mediating these effects, 3 groups of mice were evaluated: (a) high-fat diet–fed (HFD-fed) ad libitum; (b) HFD plus CANA mixed in diet (25 mg/kg/d), provided ad libitum (CANA); and (c) HFD-fed mice fed such that they were weight matched (WM) with the HFD plus CANA group, achieved via 15%–30% caloric restriction. As expected, CANA treatment induced glycosuria (Figure 1A) and reduced fasting glucose (Figure 1B) as compared with HFD ($P < 0.0001$). While fasting glucose was also decreased in WM mice, the reduction was greater in magnitude in CANA-treated mice ($P < 0.05$). CANA also attenuated HFD-induced weight gain (Figure 1C); weights of WM mice were similar to those of CANA-treated mice, as per study design. CANA-treated mice have improved oral glucose tolerance, with greater magnitude as compared with WM group (Figure 1D). Insulin levels were similar in the fasting state in all 3 groups but were lower at 15 minutes after glucose gavage in CANA-treated mice as compared with both control and WM mice (Figure 1E). Interestingly, glucose-stimulated GLP-1 levels were reduced in WM mice but were maintained in CANA-treated mice at levels similar to those of HFD-fed mice (Figure 1F). By contrast, fasting glucagon levels did not differ between groups (Figure 1G). Insulin sensitivity, assessed by insulin tolerance testing, did not differ between groups (Figure 1H). Similarly, despite lower fasting glucose with CANA, there was no change in glycemic response to glucagon or pyruvate (Supplemental Figure 1, A and B; supplemental material available online with this article; https://doi.org/10.1172/jci.insight.123130DS1). As expected, water intake was significantly increased in CANA-treated mice (Figure 1I), likely due to increased urine output through osmotic diuresis.

We hypothesized that the reduction in glucose carbon sources through glycosuria would trigger utilization of alternative fuel sources, such as fatty acids and amino acids. Indeed, metabolic cage analysis demonstrated persistently low respiratory exchange ratio (<0.7) in CANA-treated mice, even during the fed state (Figure 1J), implying increased lipid or ketone utilization, as compared with both HFD and WM mice. O_2 consumption, heat production, physical activity, and food intake were unchanged (Supplemental Figure 1, C–G). Increases in whole-body fatty acid mobilization and utilization in CANA-treated mice were also supported by a trend to increased free fatty acids (Figure 1K) and a significant increase in the serum ketones acetoacetate and 3-hydroxybutyrate (as measured by LC/MS) (Figure 1L and Supplemental Figure 1H). Serum valine, leucine, isoleucine, and total branched chain amino acids (BCAA) tended to decrease in CANA-treated mice (Supplemental Figure 1, H and I).

To further assess weight-dependent versus weight-independent effects of CANA treatment, we also analyzed in vivo metabolism in lean mice fed a low-fat diet (LFD) (Supplemental Figure 2). Similar to HFD-fed mice, CANA induced glycosuria, reduced fasting glucose, improved glucose tolerance, increased whole body lipid oxidation, and increased serum β-hydroxybutyrate levels. By contrast, CANA did not change body weight or adipose tissue mass in LFD-fed mice. Thus, metabolic responses to CANA occur even in the absence of weight loss.

CANA reduced hepatic steatosis and shifts fuel utilization from carbohydrates toward catabolic lipid metabolism and ketogenesis. To better understand the effect of CANA at a tissue level, we analyzed liver lipid metabolism. H&E staining revealed a significant reduction in hepatic steatosis in CANA-treated mice (Figure 2A); all mice in HFD group had moderate to severe steatosis, while 36% of CANA-treated mice

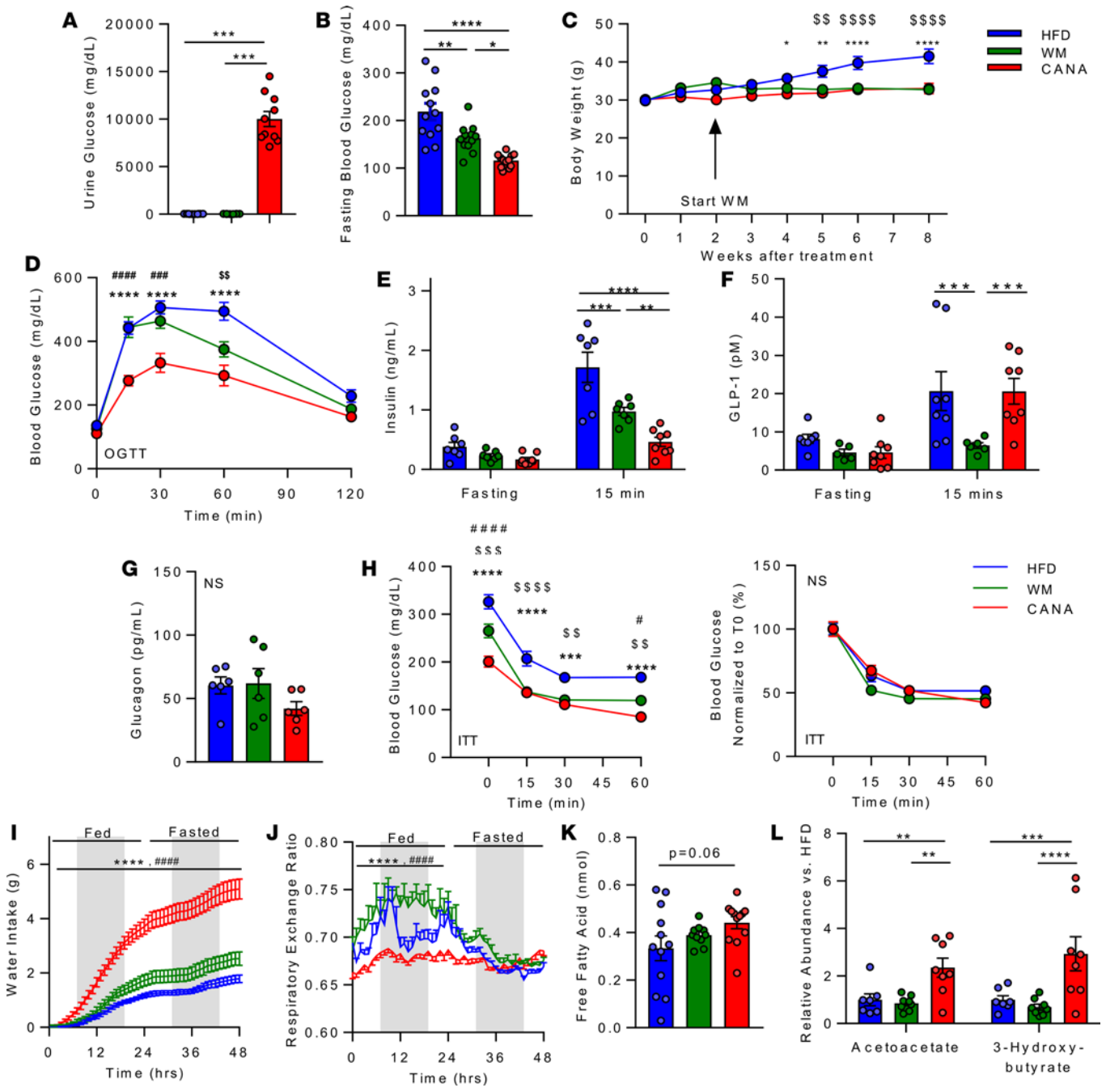

Figure 1. Canagliflozin reduces blood glucose, improves glucose tolerance, and causes a shift toward lipid utilization. (**A**) Urinary glucose in HFD, weight matched (WM), and HFD + CANA (CANA) after an overnight fast, after 8 weeks of treatment (n = 8–11/group). (**B**) Blood glucose after a 16-hour fast (n = 8/group). (**C**) Body weight (n = 12/group). (**D**) Oral glucose tolerance (2 g/kg, n = 12/group). (**E**) Plasma insulin, fasting and 15 minutes after glucose gavage (n = 8/group). (**F**) Plasma glucagon-like peptide-1 (GLP-1), fasting and 15 minutes after glucose gavage (n = 8/group). (**G**) Fasting plasma glucagon (n = 6/group). (**H**) Insulin tolerance (0.75 U/kg, n = 8/group). (**I**) Water intake (n = 6–12/group). (**J**) Respiratory exchange ratio (n = 6–12/group). (**K**) Serum-free fatty acids (4-hour fast, n = 11–12/group). (**L**) Serum ketones (LC/MS, n = 7–8/group). P values (1- or 2-way ANOVA). $^{*}P < 0.05$, $^{**}P < 0.01$, $^{***}P < 0.001$, $^{****}P < 0.0001$ in HFD vs. CANA. $^{\#}P < 0.05$, $^{\#\#}P < 0.01$, $^{\#\#\#}P < 0.001$, $^{\#\#\#\#}P < 0.0001$ in WM vs. CANA; and $^{\$}P < 0.05$, $^{\$\$}P < 0.01$, $^{\$\$\$}P < 0.001$, $^{\$\$\$\$}P < 0.0001$ in WM vs. HFD.

had no steatosis ($P < 0.0001$ vs. WM and HFD, Figure 2B). Surprisingly, there was no change in hepatic triglyceride content, as assessed by lipase hydrolysis and glycerol measurement, in CANA-treated mice, despite a significant 44% reduction in WM mice ($P < 0.01$ vs. HFD) (Figure 2C). To identify lipid species differing between HFD and CANA mice, liver samples were subjected to lipidomic analysis by LC/MS. Again, there were no changes in triglyceride content in CANA-treated mice relative to HFD-fed

mice or WM mice, nor in other lipid species, including lysophosphatidylethanolamine, lysophosphatidylcholine, phosphatidylinositol, sphingomyelin, cholesterol ester, phosphatidylethanolamine, and phosphatidylcholine (Supplemental Figure 3A). However, there was a significant 43% reduction in total diacylglycerol species (Figure 2D). In addition, there was a significant reduction in triglyceride species containing 0, 2, 3, or 4 double bonds and a significant increase in triglycerides containing 11 double bonds in CANA-treated mice (Figure 2E). While the reduction in unsaturated and monounsaturated species was observed in both WM and CANA-treated mice, the increase in polyunsaturated species was unique to CANA-treated mice. Consistent with serum patterns, 3-hydroxybutyrate was increased by 3.5-fold in CANA-treated mice but did not differ in WM mice, indicating weight loss–independent response ($P < 0.001$ for both) (Figure 2F). Cholesterol content was reduced in CANA-treated mice (27% decrease, $P < 0.05$ vs. HFD), but not in WM mice (Figure 2G).

We next assessed the effect of CANA on other metabolic pathways. Hepatic content of glycogen, the anabolic storage form of glucose, was reduced in CANA-treated mice in comparison to both HFD-fed and WM mice (55% reduction vs. HFD, 53% reduction vs. WM, $P < 0.05$ for both) (Figure 2H). Tissue metabolomics analysis revealed a robust reduction in hepatic content of multiple other metabolites, with 163 of 334 measured metabolites significantly altered (Figure 2I). Carbohydrate-derived metabolites, including glucose/fructose/galactose and 1,5-AG/1-deoxyglucose, were significantly reduced, potentially due to urinary losses of both glucose and 1,5-AG with SGLT2i (Figure 2, J and K) (12). UDP-GlcNAc, the key endpoint of the hexosamine biosynthesis pathway, and multiple glycolytic metabolites were also significantly lower in CANA-treated mice (Figure 2J). By contrast, N-carbonyl β-aminoisobutyric acid (BAIBA) and the lipidated amino acid oleoyl phenylalanine were increased; both of these have been shown to increase energy expenditure through fatty acid oxidation and uncoupling, respectively (13, 14). Metabolites upregulated in CANA-treated mice included FAD^+, AMP, ADP, NADP+, UMP, and the ketone 3-hydroxybutyric acid (Figure 2I). In addition, multiple long-chain acylcarnitine species were increased in liver, including C10, C12, C14, C16, and C18:2 (Supplemental Figure 3B). Collectively, these data indicate an overall reduction in glucose-derived metabolites, including glycogen, and a parallel increase in catabolic intermediates, including ketones. These patterns were not observed in WM mice, indicating that the effects of CANA on hepatic metabolism were weight independent.

CANA decreases mTOR signaling and activates AMPK without altering insulin and glucagon signaling. We next examined effects of CANA on hepatic signaling pathways that regulate lipid oxidative metabolism. CANA has recently been shown to activate hepatic AMPK through inhibition of mitochondrial complex I (15); in agreement, our metabolomics analysis demonstrated a significant increase in hepatic AMP (Figure 2I). Thus, we hypothesized that AMPK activation might contribute to increases in whole-body fatty acid oxidation and hepatic gene expression. Indeed, AMPK phosphorylation (threonine 172) was increased by 10-fold and 20-fold in CANA-treated and WM mice, respectively (Figure 3A). By contrast, phosphorylation of the downstream effector acetyl CoA carboxylase (Acc) was not increased, potentially due to significantly reduced total Acc protein ($P < 0.05$ vs. HFD) (Figure 3A). While lean mice treated with CANA had similar increases in lipid oxidation, AMPK and ACC phosphorylation were not increased (Supplemental Figure 4). Thus, AMPK was likely not responsible for CANA-specific increases in FA oxidation and ketogenesis.

mTOR is a cellular energetic sensor often regulated inversely with AMPK. Indeed, there was a 56% decrease in hepatic phosphorylation of the mTOR downstream substrate S6 upon refeeding in CANA-treated mice ($P < 0.05$) (Figure 3A) but not in WM controls, suggesting weight-independent reduction in mTOR signaling.

To determine whether the metabolic response to CANA was linked to alterations in tissue insulin or glucagon signaling, we analyzed multiple downstream signaling molecules using Western blot analysis of liver harvested in the fasting and refed states. There were no significant changes in phosphorylation of cyclic-AMP response elements (CREB), Akt, or forkhead box protein O1 in CANA-treated mice with fasting or refeeding (Figure 3A).

Given that diacylglycerol, an important mediator of hepatic insulin resistance, was reduced by CANA, we also assessed hepatic insulin signaling after acute inferior vena cava injection. Insulin increased phosphorylation of insulin receptor, Akt, and Gsk3, as expected; while serine phosphorylation of Akt was modestly higher in CANA-treated mice (24% increase, $P < 0.05$), there were no significant differences in insulin receptor, Akt threonine phosphorylation, or downstream glycogen synthase kinase 3 (GSK3) phosphorylation (Figure 3B). Thus insulin action is unlikely to be the driver of CANA-induced metabolic changes.

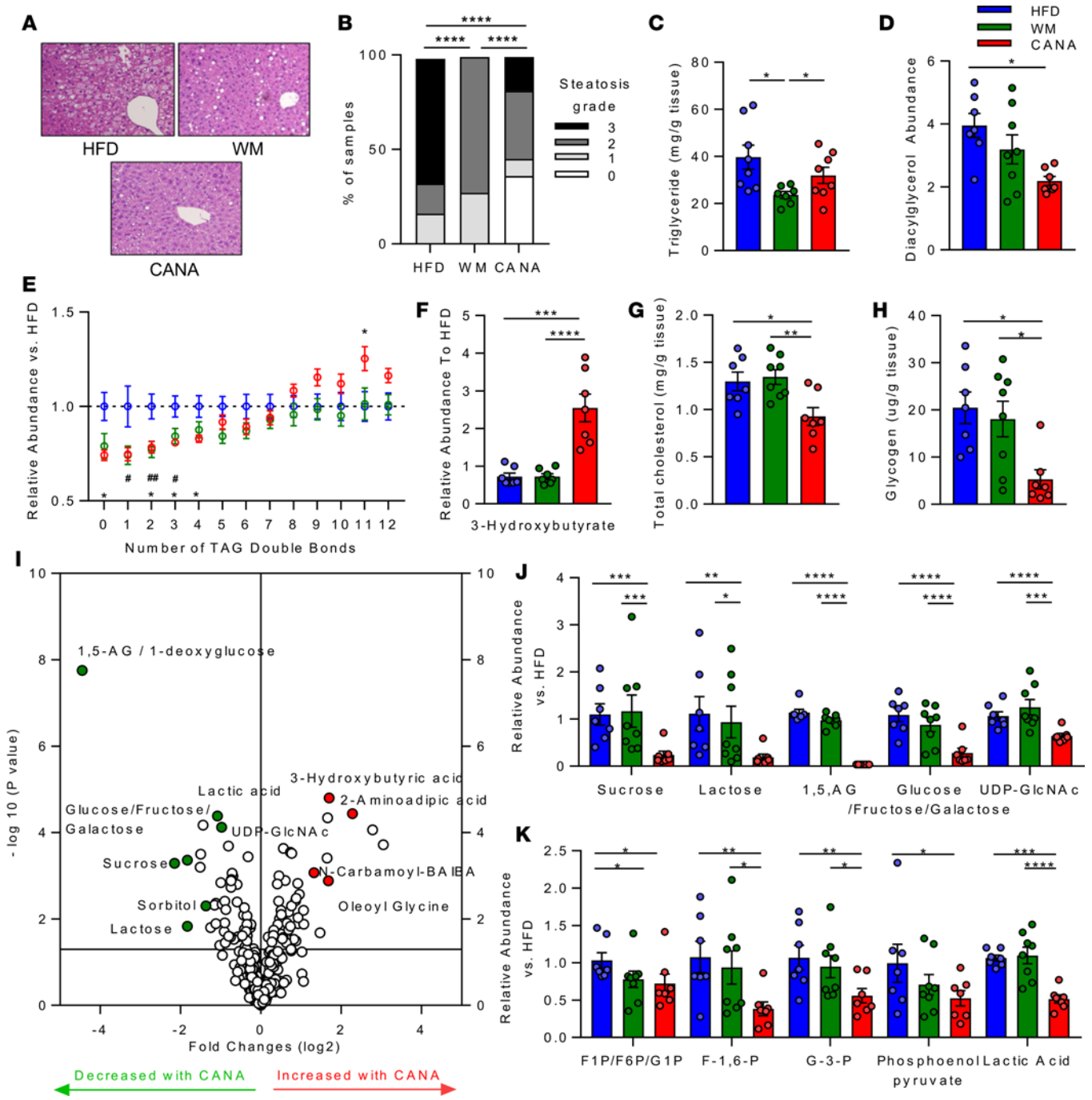

Figure 2. Canagliflozin reduced hepatic steatosis and shifts fuel utilization from carbohydrates toward catabolic lipid metabolism and ketogenesis. (**A**) Representative H&E-stained liver section. Original magnification, ×20. (**B**) Quantification of hepatic steatosis. Grade 0 indicates no steatosis, 1 indicates <33%, 2 indicates 33–66%, and 3 indicates >66% of ×20 field. (**C**) Hepatic triglyceride (n = 11–12/group). (**D**) Hepatic diacylglycerol (LC/MS). (**E**) Triglyceride content stratified by number of double bonds, normalized to the HFD group (LC/MS). (**F**) Hepatic ketones (n = 7–8/group). (**G**) Hepatic cholesterol (n = 7–8/group). (**H**) Hepatic glycogen (n = 7–8/group). (**I**) Volcano plot of hepatic metabolites altered by CANA, in comparison with HFD. (**J** and **K**) Hepatic metabolites (LC/MS, n = 7–8/group). P values (1-way ANOVA). *P < 0.05, **P < 0.01, ***P < 0.001, ****P < 0.0001.

CANA triggers transcriptional reprogramming and yields a fasting-like metabolic response and requires fatty acid oxidation for successful metabolic adaptation. To better understand the molecular mechanisms mediating the effect of CANA on hepatic metabolism, we performed microarray-based transcriptomic analysis in all 3 treatment groups. CANA treatment induced robust changes in hepatic gene expression (2522 genes differentially expressed in CANA-treated mice vs. HFD, nominal P < 0.05) (Supplemental Figure 5A). Sixteen

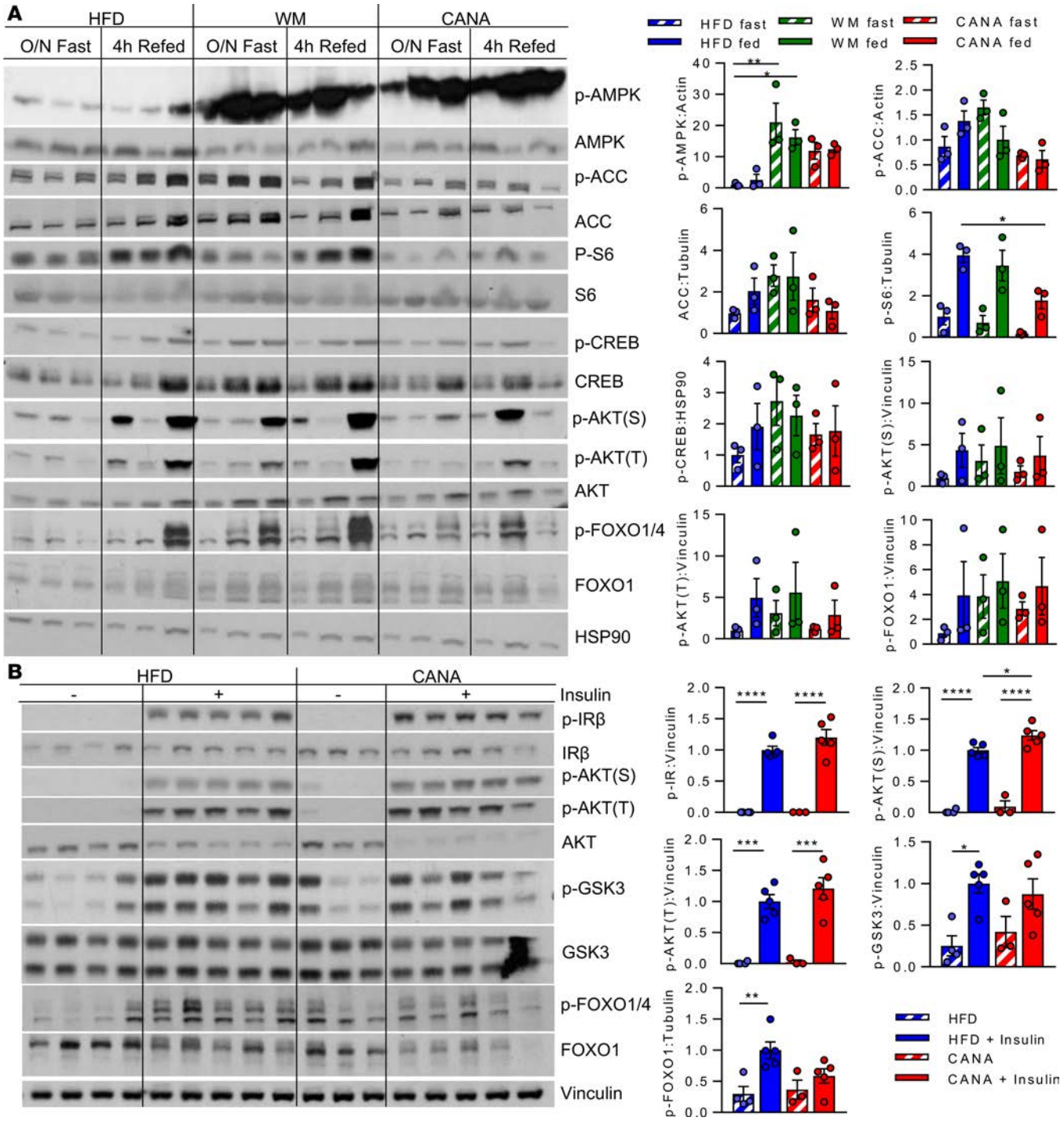

Figure 3. CANA decreases mTOR signaling and activates AMPK without altering insulin and glucagon signaling. (**A**) Phosphorylation of 5′ AMP-activated protein kinase (AMPK, Thr172), acetyl CoA carboxylase (ACC, Ser79), ribosomal protein S6 (Ser240), cAMP response element binding protein (CREB, Ser133), Akt (Thr308, Ser473), and FOXO1 (Ser256) after overnight fast with or without 4-hour refeeding. (**B**) Phosphorylation of insulin receptor IRβ (Y1135/36), Akt (Thr308, Ser473), GSK3 (Ser21/9), and FOXO1 (Ser256) in fasted or insulin-stimulated mice (5 minutes). *n* = 3–5/group. *P* values (1-way ANOVA). **P* < 0.05, ***P* < 0.01, ****P* < 0.001, *****P* < 0.0001.

transcripts were significantly altered in all comparisons ($P < 0.05$); most of these were noncoding transcripts. Pathway analysis of CANA-mediated changes revealed reduced cholesterol, de novo lipogenesis, steroid hormone, and vitamin A and D synthesis and increased tricarboxylic acid (TCA) cycle and electron transport chain pathways (all $P < 0.01$) (Supplemental Figure 5B). Genes regulating de novo lipogenesis (*Acc*, *Fasn*, and *Scd1*) were downregulated, as were genes regulating cholesterol uptake (*Pcsk9*) and syn-

thesis (*Hmgcr*, *Lss*, and *Hmgcs1*) (Figure 4A). While the glycolytic genes *Gck*, *Pgam1*, *Gapdh*, and *Pklr* were downregulated, TCA cycle and electron transport chain genes were upregulated, with increases in *Sucla2, Suclg1*, *Etfdh*, *Cycs*, *Cox5b*, and *Etfa* (Figure 4A). qPCR of selected genes confirmed expression data (Figure 4, B–F). Interestingly *Pdk4* was highly upregulated (Figure 4B), potentially contributing to reduced entry of glucose carbons into the TCA cycle. *Ppp1r3c*, a key mediator of glycogen synthesis, was also downregulated by 80% in CANA-treated mice ($P < 0.05$ and $P < 0.01$ in CANA vs. HFD and WM, respectively, Figure 4B). By contrast, expression of the gluconeogenic gene *G6pc* was increased in CANA ($P < 0.05$, Figure 4B). *Chrebp-β,* a key mediator of both carbohydrate metabolism and lipogenesis, was significantly reduced by 50% ($P < 0.05$ vs. HFD, Figure 4C). Notably, the effect of CANA treatment was consistently greater than that of limiting HFD-associated weight gain, indicating transcriptional effect to reduce glucose storage/metabolism and lipid synthesis, independent of weight loss.

Intriguingly there was no change in expression of genes encoding mitochondrial β-oxidation or ketogenesis enzymes, including *Cpt1a*, *Acadm*, *Acadl, Acadvl,* and *Hmgcs2* (Figure 4D), while the microsomal fatty acid oxidation gene *Cyp4A14* tended to increase (10-fold) in CANA (Figure 4E). There was a 2.2- and 3.6-fold increase in the regulatory nuclear receptor *Ppara* and its coactivator *Pgc1α,* respectively (Figure 4F). Transcription factor–binding site analysis identified *Ppara* as a potential transcription factor contributing to expression of upregulated genes in CANA-treated mice versus HFD-fed and WM mice (nominal $P < 0.05$) (Supplemental Figure 5C).

To test the requirement for fatty acid oxidation in CANA-induced metabolic responses, we administered etomoxir, an inhibitor of carnitine palmitoyl transporter 1 (CPT1), the major transporter of fatty acids into mitochondria. CANA-treated mice were intolerant of etomoxir, as indicated by (a) the development of hypoglycemia 60 minutes after etomoxir administration ($P < 0.001$ for CANA vs. HFD, Supplemental Figure 6A) and (b) subsequent 100% mortality ($P < 0.03$ for CANA vs. HFD, Supplemental Figure 6B). Thus, these data support the hypothesis that fatty acid oxidation is required for successful adaptation to CANA.

CANA triggers coordinated interorgan nutrient repartitioning from adipose tissue. CANA-induced increases in fatty acid oxidation and ketogenesis could reflect observed reductions in glucose availability and metabolism as well as increased systemic flux of lipids from adipose tissue linked to reduced insulin levels (Figure 1E). Indeed, subcutaneous and gonadal fat mass were reduced in both CANA-treated and WM mice, while brown adipose weight was reduced only in CANA-treated mice (Figure 5A and Supplemental Figure 4A). We further observed a significant reduction in the mean size of subcutaneous adipocytes (Figure 5, B and C). To test whether adipose lipolysis could contribute to these findings, we stimulated mice in vivo with the β-3 adrenergic agonist CL-316243. Free fatty acid release in response to CL-316343 was increased by 3-fold in CANA-treated mice, as compared with 2-fold increase in HFD-fed mice ($P < 0.05$ between groups, Figure 5D). There was no increase in *Ucp1* expression or other markers of browning (Figure 5E), there was no change in adiponectin levels (Supplemental Figure 7B), and there were no differences in thermogenic responses to cold exposure between groups (Supplemental Figure 7C and Supplemental Methods). Quantification of islet size revealed a significant reduction in both CANA-treated and WM mice (Supplemental Figure 7, D and E). Thus, adipose effects were more pronounced in CANA-treated mice than in WM controls, supporting CANA-mediated promotion of white adipose lipolysis, potentially mediated by reduced insulin levels.

CANA increases hepatic and serum FGF21. Since CANA had marked effects suggesting partitioning of nutrients away from adipose tissue and toward liver for oxidation, we hypothesized that the hepatokine FGF21 could be orchestrating CANA-mediated whole-body metabolic shifts. Indeed, CANA-treated mice had significant increases in both hepatic Fgf21 mRNA expression (3.9-fold, $P < 0.05$, Figure 6A) and fasting serum FGF21 levels (2.2-fold higher than HFD-fed mice: 6223 ± 373 vs. 2784 ± 536 pg/ml, $P < 0.05$); increased plasma FGF21 was not observed in WM controls (Figure 6B). These patterns were potentially mediated by increased *Ppara* and *Pgc1α,* respectively (Figure 4F). Taken together, these data indicate that CANA triggers a fasting-like catabolic switch, increasing adipose lipolysis, hepatic fatty acid oxidation, and ketogenesis, potentially via FGF21-dependent mechanisms.

FGF21 is not required for CANA-induced effects on glucose tolerance, hepatic lipid metabolism, and steatosis. FGF21 is a fasting-induced hepatokine that can trigger whole-body metabolic switch from glucose to fatty acid utilization (16). Given that both plasma concentration and hepatic expression of *Fgf21* were increased in response to CANA, we tested the requirement for FGF21 in mediating metabolic effects of CANA using mice fed a 60% HFD. HFD-fed FGF21 whole-body-KO (FGF21-KO) mice and WT controls were treated with CANA for 6 weeks. CANA treatment induced a massive increase in urine glucose, as expected, but glycosuria was slightly greater in FGF21-KO mice ($P < 0.0001$, CANA-treated WT vs. FGF21 KO) (Figure 7A). FGF21-KO and WT

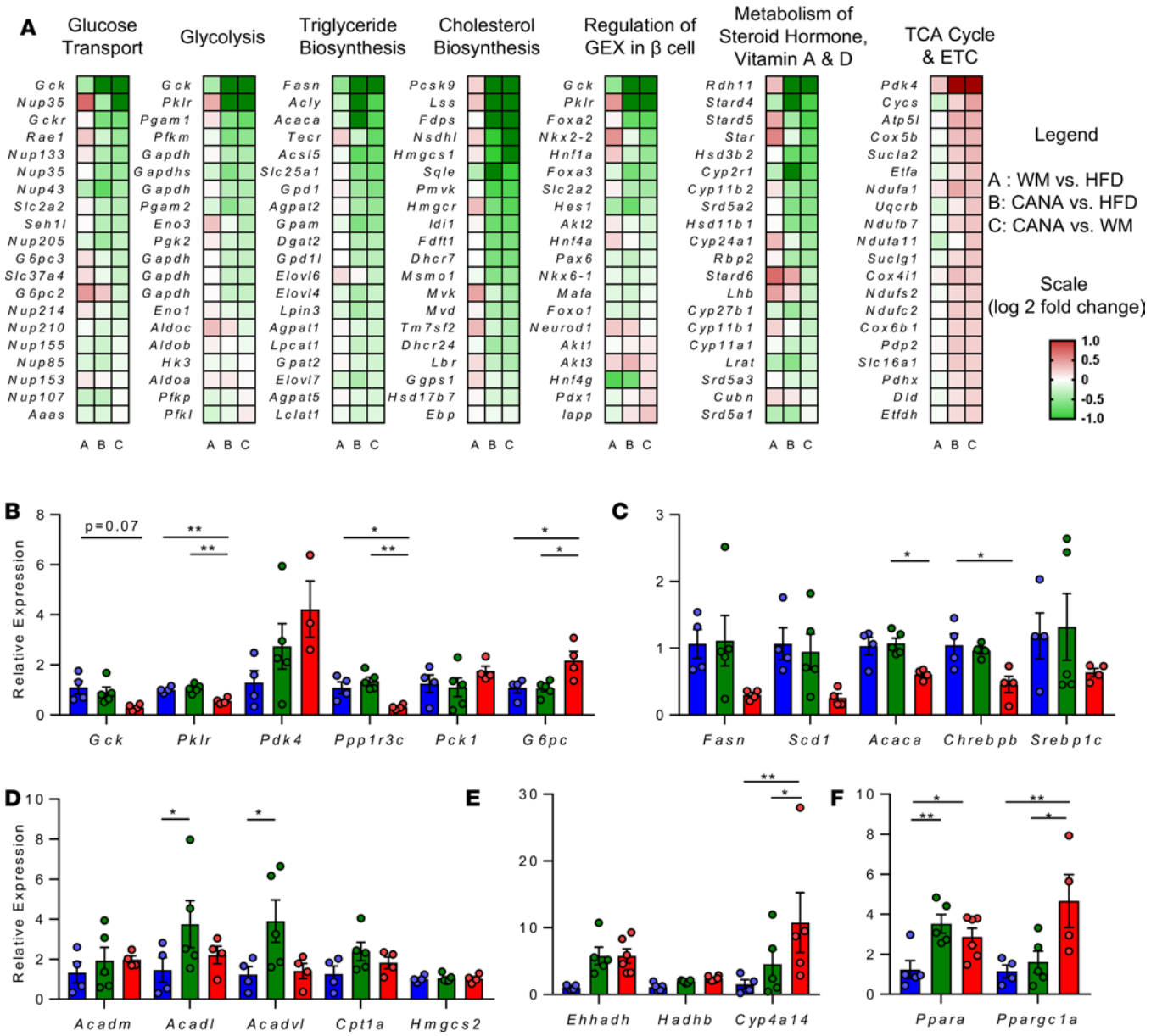

Figure 4. Canagliflozin triggers transcriptional reprogramming, reflecting a fasting-like metabolic state. (**A**) Heatmap of individual genes within selected pathways, colored by $\log_2$ fold change. (**B**–**F**) qPCR validation of selected genes (n = 3–5/group). P values (1-way ANOVA). $^*P < 0.05$, $^{**}P < 0.01$.

mice had a similar reduction in fasting blood glucose in response to CANA (Figure 7B). Although FGF21-KO mice were more glucose intolerant than WT mice at baseline, they had similar-magnitude improvement with CANA (Figure 7C). Insulin sensitivity was not affected by CANA in either genotype (Figure 7D).

Since FGF21 is an important mediator of whole-body and hepatic adaptation to ketogenic diet (16), we tested whether FGF21 is also required for CANA-induced ketogenesis. Interestingly, CANA lowered the respiratory exchange ratio by a similar magnitude in both FGF21-KO and WT mice (Figure 7E). Likewise, CANA induction of β-hydroxybutyrate was similar in both FGF21-KO and WT mice (Figure 7F). Similar to the original cohort, there was no change in O_2 consumption, heat production, physical activity, or food intake in either WT or FGF21-KO mice (Supplemental Figure 8, A–E). At a tissue level, hepatic steatosis was worse in FGF21-KO mice at baseline, but CANA improved steatosis to a similar extent in both WT and FGF21-KO mice (Figure 7G).

As expected, *Fgf21* expression was absent in FGF21-KO mice (Supplemental Figure 8F). Hepatic expression of *Ppara* and *G6pc* was higher in FGF21-KO mice at baseline, but there was no additional

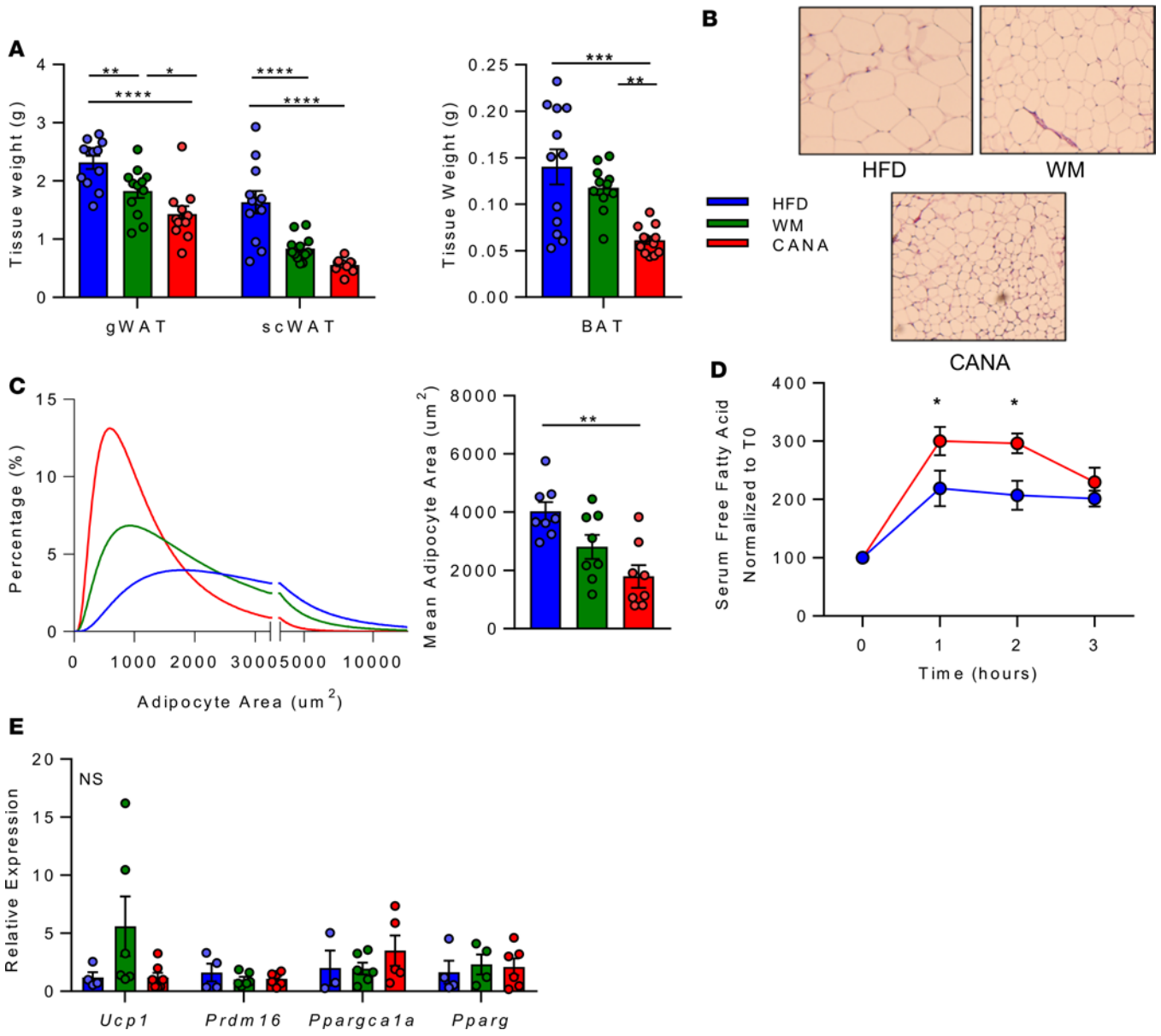

Figure 5. Canagliflozin triggers coordinated interorgan nutrient repartitioning from adipose tissue. (**A**) Tissue weight after 9 weeks of CANA (n = 12/group). gWAT, perigonadal; SC, subcutaneous; BAT, brown adipose tissue. (**B**) Representative H&E-stained subcutaneous adipose section. Original magnification, ×40. (**C**) Quantification of adipocyte size (n = 8/group). (**D**) Percentage change in free fatty acids after CL-316243 injection (0.1 mg/kg, n = 6/group). (**E**) qPCR analysis of subcutaneous adipose gene expression after 4 hour fast (n = 6/group). P values (1-way ANOVA). *P < 0.05, **P < 0.01, ***P < 0.001, ****P < 0.0001.

incremental response to CANA (Figure 7, H and I). Expression of glucose and lipogenic regulatory genes, including *Gck*, *Chrebp-β*, and *Fasn*, was similarly reduced in both WT and FGF21-KO mice treated with CANA (Figure 7I). Thus, CANA-induced increases in whole-body fatty acid metabolism, ketogenesis, and hepatic transcriptional reprograming are independent of FGF21.

FGF21 is required for effects of CANA on body weight and induction of adipose lipolytic transcriptional regulation. WT mice treated with CANA had lower body weight as compared with untreated controls. FGF21-KO mice treated with CANA had a trend toward higher body weight as compared with WT mice treated with CANA (Figure 8, A and B). Moreover, there was a paradoxical increase in gonadal white adipose (gWAT) tissue weight in FGF21-KO mice treated with CANA (Figure 8C), despite similar trends for CANA to reduce subcutaneous weight in both genotypes (Figure 8C). Adipocyte size in gWAT of untreated WT and FGF21-KO mice had similar distributions; by contrast, CANA reduced mean adipocyte size in WT mice but actually

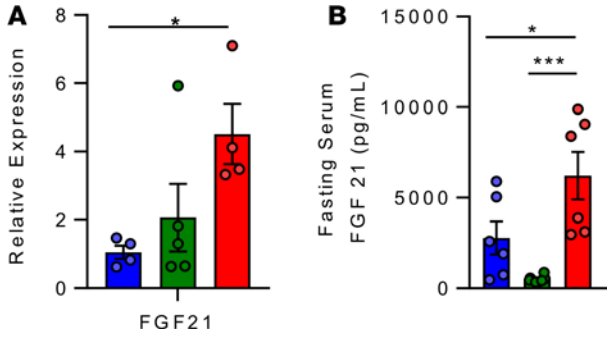

Figure 6. Canagliflozin increases hepatic and serum FGF21. (**A**) Hepatic expression of *FGF21* after a 4-hour fast (n = 3–5/group). (**B**) Fasting serum FGF21 level, as measured by ELISA (n = 6/group). P values (1-way ANOVA). *P < 0.05, **P < 0.01, ***P < 0.001.

increased mean adipocyte size in FGF21-KO mice (Figure 8, D and E). Indeed, mean adipocyte area was increased by 1.6-fold in CANA-treated FGF21-KO versus CANA-treated WT mice (P < 0.05, Figure 8F).

FGF21 can act in the central nervous system to induce sympathetic nervous system activation, energy expenditure, and weight loss (17, 18). Sympathetic activation is also required for the maximal weight loss effect of a ketogenic diet (19). As sympathetic activation is critical for induction of lipolysis in white adipose tissue, we hypothesized that defective lipolysis might contribute to a reduced CANA effect on weight loss, adiposity, and cell size in FGF21-KO mice. Indeed, expression of β-3 adrenergic receptor (β3ar) and adipose triglyceride lipase (*Atgl*) was upregulated by 2.2-fold in WT mice treated with CANA. However this upregulation was abolished in FGF21-KO mice treated with CANA (P < 0.05, Figure 8G). In addition, Atgl was also significantly upregulated by 3.6-fold at the protein level (P < 0.05, Figure 8I). There was no change in mRNA expression of other lipolytic enzymes, such as hormone-sensitive lipase (*Hsl*) or monoglyceride lipase (*Mgll*). In addition, expression of the deiodinase type 2 (*Dio2*), another target of sympathetic activity, was reduced by 77% in FGF21-KO mice, in both CANA-treated and untreated states (P < 0.05, Figure 8G). Gene expression analysis also revealed differential regulation by CANA for regulators of lipogenesis, with upregulation of *Acc* and *Dgat1* by 2.2- and 2.7-fold in WT mice but no induction in FGF21-KO mice; similar trends were observed for *Chrebp* (Figure 8H). Interestingly, there was no alteration in expression of *Pparg* (Supplemental Figure 9A), but expression of *Ppard* was reduced in FGF21-KO mice in both treated and untreated states (P < 0.05, Figure 8H). In addition, phosphorylation of HSL, a key regulator of lipolysis, was significantly higher in CANA-treated mice (10-fold vs. untreated, P < 0.05). Notably, the CANA-induced increase in HSL phosphorylation was abolished in FGF21-null mice (HSL phosphorylation 87% lower in CANA-treated FGF21-null vs. WT mice, P = 0.06, Figure 8I). Thus, Fgf21 appears to be essential for CANA-induced reduction of adipose tissue mass, adipocyte cell size, and activation of lipolysis programming at a transcriptional and protein level.

Discussion

SGLT2i have recently been demonstrated to reduce both overall and cardiovascular mortality in T2D (3). While alterations in both hemodynamic and metabolic regulation have been hypothesized as mediators of these beneficial effects, the precise mechanisms remain unknown. Identification of molecular regulators governing the metabolic effect of cellular and systemic glucose reduction will not only facilitate our understanding of SGLT2i pharmacology, but may also contribute to development of novel therapies or predictors of responses.

We now demonstrate that urinary glucose loss through SGLT2i not only reduces blood glucose and improves glucose tolerance, but also triggers a robust metabolic switch from using glucose carbon as fuel toward a fasting-like state, with increased fatty acid utilization and ketogenesis. This fuel mobilization also reduced liver steatosis, lipogenesis and adipose tissue mass. Importantly, these findings were not observed in weight-matched controls but were consistent even in lean animals, indicating these effects are independent of weight loss and instead reflect additional metabolic consequences of SGLT2i and urinary glucose loss.

With marked reductions in glucose availability and utilization, alternative fuel sources must be utilized to supply the TCA cycle during fasting, such as amino acids (20–22) or fatty acids. We found only modest reductions in all 3 circulating BCAA, and no significant changes in expression of genes regulating

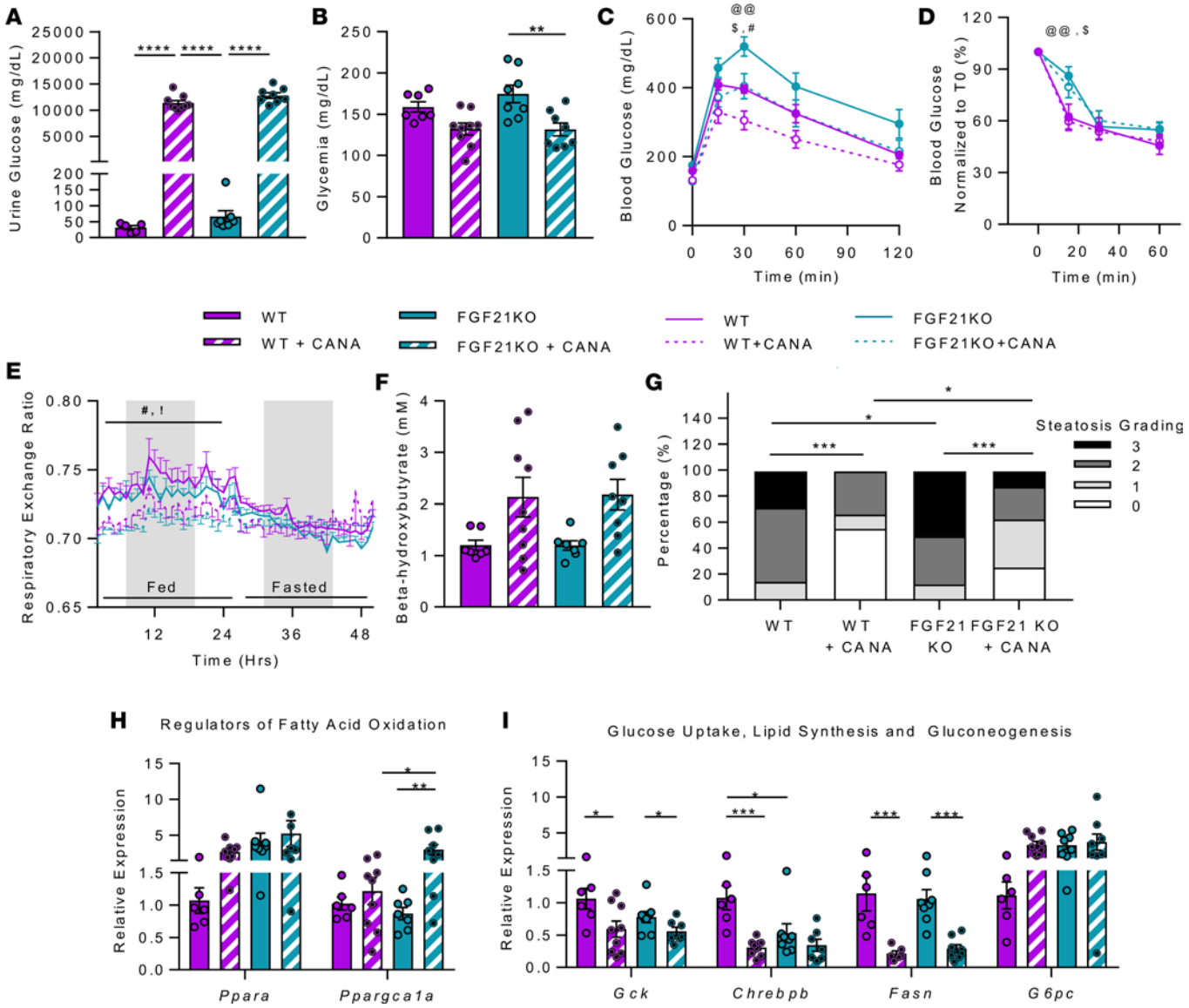

Figure 7. FGF21 is not required for CANA-induced improvement in glucose tolerance, activation of fatty acid oxidation and ketogenesis, reduction in hepatic steatosis, and transcriptional reprogramming. (**A**) Urinary glucose after 6 weeks of CANA (n = 6–9/group). (**B**) Blood glucose, random fed (n = 7–9/group). (**C**) Intraperitoneal glucose tolerance test (1 g/kg) after overnight fast (n = 7–9/group). (**D**) Insulin tolerance test (n = 7–9/group). (**E**) Respiratory exchange ratio (n = 7–9/group). (**F**) Serum ketones after 16-hour fast (n = 7–9/group). (**G**) Quantification of hepatic steatosis by histology scoring. (**H** and **I**) qPCR of regulatory genes for fatty acid oxidation, ketogenesis, glucose metabolism, lipogenesis, and gluconeogenesis in liver (n = 6–8/group). P values (1- or 2-way ANOVA). $^{*}P < 0.05$, $^{**}P < 0.01$, $^{***}P < 0.001$, $^{****}P < 0.0001$; $^{@@}P < 0.01$ in WT vs. FGF21 KO; $^{!}P < 0.05$ in WT vs. WT + CANA; $^{\#}P < 0.05$ in FGF21 KO vs. FGF21 KO + CANA; $^{\$}P < 0.05$ in WT+ CANA vs. KO + CANA.

amino acid catabolism. Instead, our data point to an important role for lipid metabolism as mediator of the hepatic and systemic metabolic shift observed with CANA, as indicated by altered lipid composition, increased ketones, upregulation of genes promoting lipid oxidation and TCA cycle activity, and reduction in lipogenic gene expression. Interestingly, there was an increase in polyunsaturated lipids, particularly for triglycerides with >9 double bonds. This pattern, which was unique to CANA and not observed in WM mice, is similar to the serum triglyceride composition previously linked to metabolic health and decreased progression from impaired fasting glucose to T2D in humans (23). Moreover, CANA reduced hepatic levels of diacylglycerols, previously linked to hepatic insulin resistance (24).

Glucose-responsive nutrient sensors could contribute to metabolic shifts induced by CANA. For example, CANA reduced hepatic levels of UDP-GlcNAc, the end-product of the glucose-sensing hexosamine biosynthetic pathway. However, we observed no difference in GlcNAc posttranslational protein modifica-

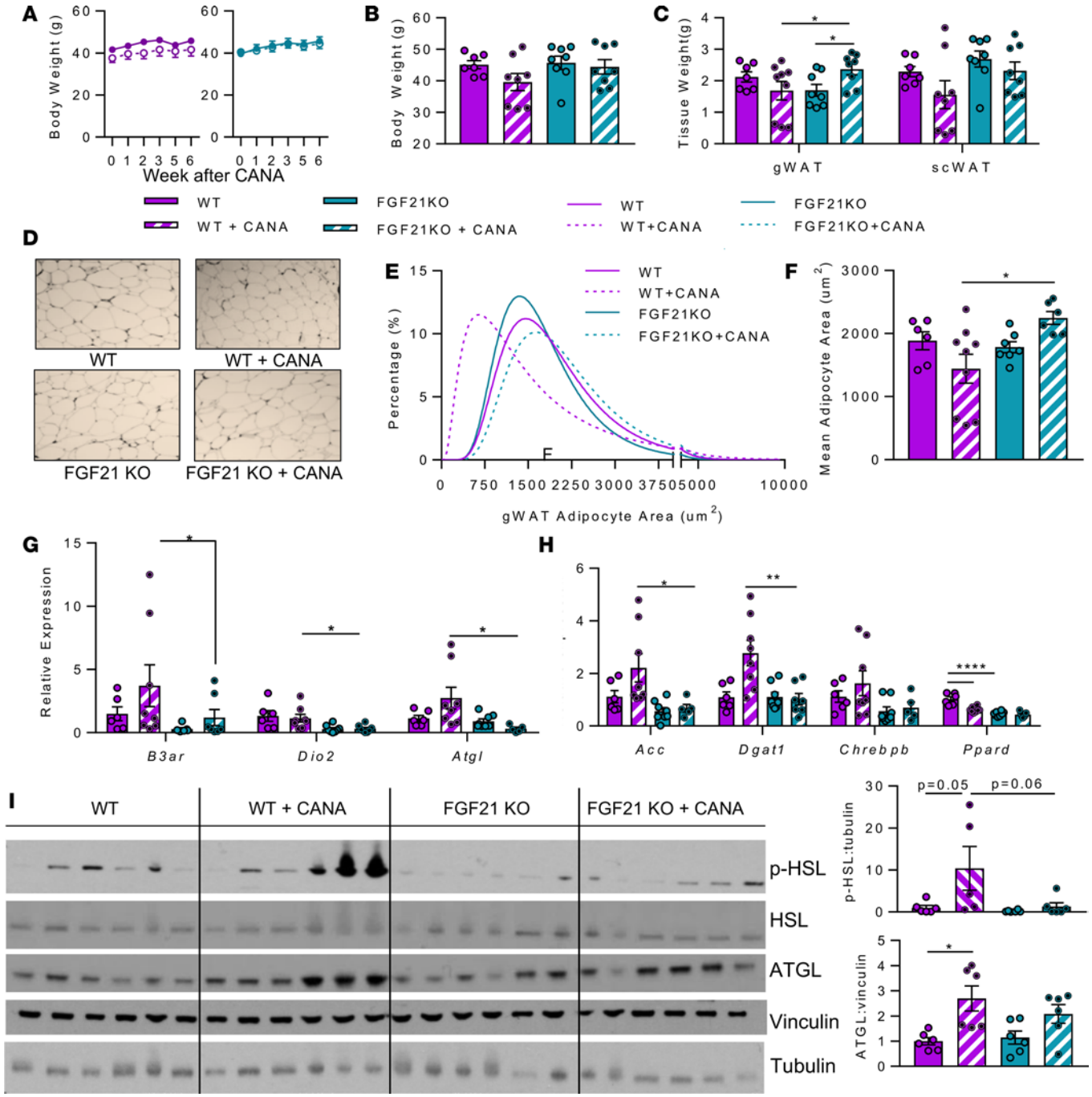

Figure 8. FGF21 is required for CANA-induced reduction in adipocyte size and activation of sympathetic and lipolysis-related gene expression. (**A**) Body weight (n = 7–9 animals/group). (**B**) Body weight after 6 weeks of treatment (n = 7–9 animals/group). (**C**) Tissue weight after 6 weeks of CANA treatment (n = 7–9/group). (**D**) Representative H&E-stained gonadal adipose section. Original magnification, ×10; scale bar: 100 μM. (**E**) Adipocyte area histogram (n = 7–9/group). (**F**) Mean adipocyte size (n = 7–9/group). (**G** and **H**) qPCR of genes regulating oxidative phosphorylation, sympathetic activation, and adipose function (n = 6–7/group). (**I**) Western blot and quantification of hormone-sensitive lipase (HSL) (Ser660 and total protein) and adipose- triglyceride lipase (ATGL) (n = 6/group). P values (1 or 2-way ANOVA). *P < 0.05, **P < 0.01, ***P < 0.001, ****P < 0.0001.

tion (data not shown) (25). Chrebp-β, which can be activated by glucose to increase glycolysis and lipogenesis, was robustly suppressed with CANA. However, ChREBP suppression alone is not sufficient to activate fatty acid oxidation, ketogenesis, and gluconeogenesis (26, 27).

AMPK is a nutrient sensor coordinating the balance between anabolism and catabolism. Intracellular AMP content and hepatic AMPK phosphorylation were increased with CANA in obese mice. While increased activation of AMPK was also observed by Hawley et al., AMPK was not required for CANA

effects to reduce glucose and increase fatty acid oxidation (15). In agreement, our data indicate that AMPK activation by CANA is not consistently linked to metabolic efficacy of the drug. For example, AMPK is not activated in lean mice treated with CANA, despite action of the drug to reduce glucose and activate lipid oxidation; conversely, AMPK is similarly activated in weight-matched and CANA-treated obese mice, despite differential metabolic responses. Such context-specific activation of AMPK dissociated from metabolic response indicates that it is not likely the major mediator of CANA-induced metabolic responses.

We also considered the possible effect of hormonal responses as mediators of CANA-mediated metabolic adaptations. Insulin levels were reduced in CANA-treated mice, and hepatic signaling was not markedly altered in CANA-treated mice, suggesting insulin action was not responsible for metabolic adaptations. SGLT2i treatment increases glucagon levels in humans with T2D, potentially via direct effects in α cells (5, 8, 28). However, plasma glucagon levels, glucagon responsiveness, and tissue activation of CREB were not altered in our model. Consistent with our findings, plasma glucagon is unchanged with SGLT2i treatment in some studies of rodents with either T1D or T2D (29). Collectively, these data indicate that increased glucagon signaling is not a uniform effect of SGLT2i and that neither insulin nor glucagon are sufficient to coordinate SGLT2i-induced metabolic shifts in nondiabetic rodents.

Our data indicate potent effects of CANA to increase hepatic expression of FGF21, yielding increases in serum FGF21 levels even higher than those in HFD-fed mice, findings consistent with increased FGF21 in SGLT2i-treated mice recently reported by Xu et al. (30). FGF21 is activated in response to prolonged fasting or nutritional ketosis (31), in part via peroxisome PPARα binding to its promoter, and is required for maximal induction of adipose tissue lipolysis, hepatic fatty acid oxidation, ketogenesis, and gluconeogenesis (31, 32). FGF21 can also induce thermogenesis by triggering a futile cycle of lipogenesis, lipolysis, and oxidative phosphorylation in adipose tissue. This can occur via either adipose FGFR/β-klotho receptor signaling or centrally mediated activation of the sympathetic nervous system (17, 18, 33–37). Since these effects mirror multiple metabolic effects of SGLT2i, we hypothesized that FGF21 would also mediate CANA-induced metabolic effects.

Interestingly, we now report that FGF21 is not required for either CANA-mediated improvement in glucose tolerance or induction of a broad fasting-like catabolic transcriptional program. At a whole-body level, CANA similarly lowered RQ in both WT and FGF21-KO mice, indicating similar shifts toward lipid metabolism. Moreover, plasma ketones are similarly increased in FGF21-KO mice treated with CANA. Both PPARα and PPAR γ coactivator 1-α (PGC1α) were increased in liver, independent of FGF21. Thus, CANA-induced increases in whole-body and hepatic lipid oxidative metabolism, ketogenesis, and transcriptional regulation are FGF21-independent. CANA-mediated reduction in glycogen could play a direct role in activating ketone synthesis (38) and regulating sympathetic activation of adipose lipolysis (39); reductions in Tor-dependent signaling could also activate PPARα-dependent ketogenesis (40). Moreover, acetylation or other posttranslational modifications of mitochondrial proteins or transcription factors could play an additive role to activate PPARα, fatty acid oxidation, and ketogenesis (41, 42). Likewise, the direct effect of intermediary metabolites, especially glucose, on chromatin structure could contribute to the control of cellular function and metabolism (43). Testing these possibilities will be important in the future.

By contrast, our data indicate that FGF21 is required for weight loss and effects of SGLT2i on adipocyte metabolism. While CANA reduced adipocyte size, FGF21-null mice had no weight loss, and adipose tissue and cell size actually increased in response to CANA. At a transcriptional level, FGF21-null mice failed to upregulate expression of the β3-adrenergic receptor or *Atgl* in response to CANA. Similarly, ATGL protein expression and Hsl phosphorylation failed to increase in CANA-treated FGF21-null mice, suggesting impaired sympathetic and lipolytic activity. This is not surprising as FGF21 increases oxidative metabolism, browning, and lipolysis in white adipose tissue (18, 31, 44) via either direct interaction with β-klotho or via activation of the sympathetic nervous system or immune cells (17). Interestingly, recent studies have also demonstrated that sympathetic activation is also critical for weight loss in the context of nutritional ketosis (19). Future work will identify whether FGF21 per se, or FGF21-dependent activation of sympathetic nervous system signaling, is required to mediate weight loss with SGLT2i therapy. We acknowledge limitations of our study. First, measures of in vivo physiology together with metabolomic and transcriptomic data suggest that CANA induces shifts in nutrient metabolism but do not permit direct assessment of metabolic fluxes. While the dose of CANA used in our study yields plasma drug concentrations (10 μg/ml) that are similar to levels achieved in humans after a typical 300 mg clinical dose (3.4–4.6 μg/ml) (data provided by Janssen Pharmaceuticals), findings in mouse models may not mirror dose-response relationships in humans. Moreover, findings in rodent models may not be fully generalizable to human pathophysiology.

In summary, we found that reduction in whole-body and tissue glucose via treatment of diet-induced obese mice with the SGLT2i CANA induced robust metabolic and transcriptomic reprogramming. Modulation of the PPARα-FGF21 axis, reduced insulin concentrations, and altered activity of cellular nutrient sensors yield a fasting-like catabolic state. Hepatic reprogramming of metabolism and transcription does not require FGF21, but FGF21 is required for CANA-mediated reduction in adiposity and activation of lipolysis.

Methods

Animal husbandry. Six-week-old C57BL6/J male mice were obtained from Jackson Laboratories. Animals were maintained at 22°C ± 2°C on a 12-hour light/dark cycle, with ad libitum access to water and food unless otherwise indicated. Three experimental groups were assessed: (a) HFD ad libitum (60% kcal from fat, Research Diets, D12492); (b) HFD plus CANA mixed in diet (25 mg/kg/d), fed ad libitum; or (c) HFD, weight matched to CANA (WM), achieved via 15%–30% caloric restriction. For the LFD study, mice were fed either LFD (10% kcal from fat, Research Diet, D12450J) ad libitum or LFD mixed with CANA (25 mg/kg/d). Food consumption and body weight were monitored weekly. Mice were sacrificed using pentobarbital (50–100 mg/kg) after a 4-hour or overnight fast with 4-hour refeeding, as indicated.

FGF21-KO mice were originally generated at Eli Lilly Research Laboratory, as previously reported (32). Briefly, targeted disruption of the Fgf21 locus resulted in deletion of the 3′ portion of exon 1, all of exon 2, and the 5′ region of exon 3. Founder mice were subsequently backcrossed onto the C57BL6/J line for at least 10 generations.

Metabolic testing. Oral glucose tolerance tests were conducted after a 16-hour overnight fast and gavage with glucose (1 g/kg body weight). For intraperitoneal glucose and pyruvate tolerance tests, mice were fasted for 16 hours before injection (2 g/kg glucose, 1 g/kg pyruvate). Blood glucose was measured at indicated time points using the Presto glucometer. Insulin, glucagon, CL316243, and etomoxir responsiveness were assessed after a 4-hour fast and injection of insulin (0.75 U/kg Humulin R, Lilly), glucagon (20 μg/kg, Lilly), CL316243 (0.1 mg/kg), and etomoxir (15 mg/kg). Resting energy expenditure, VO_2, VCO_2, food intake, and activity were measured in Comprehensive Laboratory Animal Monitoring System as previously described (CLAMS, Columbus) (18).

Transcriptomics and PCR. Total RNA was isolated from tissues harvested from mice treated for 4 weeks in each of the 3 experimental groups (n = 3–5 per group) using TRIzol (Life Technologies) and processed for hybridization to Affymetrix Mouse ST 2.0 as described previously (45). Real-time quantitative PCR was performed using SYBR green detection (Bio-Rad) in a PRISM 7900 Sequence Detection System (Applied Biosystem). Primer sequences are listed in Supplemental Table 1. The data were normalized using robust multiarray average.

Metabolomics and lipidomics. Tissues harvested after 4 weeks of treatment were used for analysis of plasma and liver metabolites, using liquid chromatography–mass spectrometry (LC/MS) to determine metabolites, lipid class, and specific lipid content (46). Missing data were imputed with half of the minimum intensity of the metabolite, and the imputed data were quantile normalized and $\log_2$ transformed.

Serum hormones and liver parameters. Plasma insulin (Crystal Chem, 90080), GLP-1 (Crystal Chem, 81508), FGF21 (R&D Systems, MF2100), adiponectin (R&D Systems, MPR300), and glucagon (R&D Systems, DGCG) were measured by ELISA. Liver lipids were extracted by chloroform/methanol prior to quantification of triglycerides and cholesterol using a colorimetric assay (Cayman Chemical, 10010303, and Cell Biolabs, STA-384). Liver glycogen was measured following manufacturer's instructions (MilliporeSigma, MAK016).

Histology. Liver, subcutaneous fat, and pancreas were isolated, weighed, and fixed in 10% buffered formalin (Fisher). Paraffin-embedded sections were stained with H&E. Images were captured using a digital camera coupled to an optical microscope (Olympus). Steatosis score was assessed at ×20 magnification and graded from 0–3: 0 (no steatosis), 1 (<33% of field), 2 (33%–66%), or 3 (>66%). For islet and adipocyte quantification, at least 100 adipocytes and islets were measured from mouse pancreatic or subcutaneous adipose sections and quantified using ImageJ (NIH).

Western blotting. Liver samples harvested after 4 weeks of treatment were homogenized using TissueLyser (Qiagen) in ice-cold lysis buffer with protease and phosphatase inhibitors (10 mM Na orthovanadate, 2 mM phenylmethylsulfonyl fluoride, 20 mM leupeptin, 2 mM benzamidine, 1.5 mM aprotinin) and spun at 14,000 *g* for 20 minutes at 4°C. Protein content was measured using a bicinchoninic acid (BCA) assay. Liver extracts containing 20 μg protein were separated by SDS-PAGE (4%–12% Bis-Tris gel, NuPAGE). Proteins were transferred to nitrocellulose and were blocked with StartingBlock (Thermo

Scientific, 37539) prior to overnight incubation at 4°C with primary antibody, as indicated. All antibodies were purchased from Cell Signaling Technologies and used at 1:1000 dilution, unless otherwise specified: pAMPK (no. 2535), AMPK (no. 2532), pACC (no. 3661), ACC (no. 3662), pS240/244 s6 (no. 2215), S6 (no. 2217S), pT308 Akt (no. 9275), pS473 Akt (1:500, no. 9271), Akt (no. 9272), pFoxo1 (no. 9461), Foxo1 (no. 2880S), pS133 CREB (no. 9191), CREB (no. 9197), pHSL (no. 4139), Hsl (no. 4107), and Atgl (no. 2138). After washing in TBS/T, membranes were incubated for 1 hour at room temperature with HRP-conjugated goat anti-rabbit secondary antibody. Proteins were detected using enhanced chemiluminescence (Lumiglo). After stripping with 2-mercaptoethanol, blots were reprobed with anti-β-actin (no. 3700) or α-tubulin (no. 3873) antibodies. Band intensities were quantified using Image J (NIH).

Bioinformatic analysis. For liver transcriptomics and metabolomics data sets, principal component analysis revealed that the first principal component was an extraneous source of variation, so it was accounted for as a covariate in linear modeling (47). Metabolomics/lipidomics sample weights were unbiasedly estimated (48) and used in linear modeling. Linear modeling differential analysis was done with the R package limma (49). Nominal *P* values were corrected for multiple testing using the FDR. Transcriptomic pathway and transcription factor prediction analysis was done using the Roast method (50), with pathways defined by Reactome and TFT database (51).

Statistics. Values are presented as mean ± SEM. Statistical analyses were performed using GraphPad Prism 7, using ANOVA followed by Tukey test for comparison of more than two groups. $P < 0.05$ was considered significant.

Study approval. All experiments were conducted as stated in the NIH *Guide for the Care and Use of Laboratory Animals* (National Academy Press, 1996) and approved by the Joslin Diabetes Center and Beth Israel Deaconess Medical Center Institutional Animal Care and Use Committees.

Author contributions

SO, CM, and MEP designed the study, generated data, and wrote the manuscript. SO, CM, VS, CK, JCW, and YT conducted the experiments. GS provided FGF21-null mice and assisted with the design and implementation of the in vivo experiments in FGF21-null mice. JM and RG performed the LC/MS metabolomics experiments and assisted with interpretation. JMD and HP performed the bioinformatics analysis. All authors reviewed and edited the manuscript.

Acknowledgments

We are especially grateful to Eleftheria Maratos-Flier for her valuable contributions to studies of the FGF21-KO mice. We thank Grace Daher (Joslin Diabetes Research Center Molecular Phenotyping Core) for performing microarray analysis. We thank members of the Patti lab for helpful discussion. We are grateful for investigator-initiated research support and the supply of CANA from Janssen Research and Development. SO is grateful for funding from the Prince Mahidol Award Foundation under the Royal Patronage. We acknowledge support from the Joslin Diabetes Research Center (P30 DK036836).

Address correspondence to: Mary-Elizabeth Patti, Room 620, Joslin Diabetes Center, 1 Joslin Place, Boston, Massachusetts 02215, USA. Phone: 617.309.1966; Email: mary.elizabeth.patti@joslin.harvard.edu.

1. Cefalu WT, et al. Efficacy and safety of canagliflozin versus glimepiride in patients with type 2 diabetes inadequately controlled with metformin (CANTATA-SU): 52 week results from a randomised, double-blind, phase 3 non-inferiority trial. *Lancet*. 2013;382(9896):941–950.
2. Rosenstock J, et al. Dose-ranging effects of canagliflozin, a sodium-glucose cotransporter 2 inhibitor, as add-on to metformin in subjects with type 2 diabetes. *Diabetes Care*. 2012;35(6):1232–1238.
3. Neal B, Perkovic V, Matthews DR. Canagliflozin and cardiovascular and renal events in type 2 diabetes. *N Engl J Med*. 2017;377(21):2099.
4. Ohki T, Isogawa A, Toda N, Tagawa K. Effectiveness of ipragliflozin, a sodium-glucose co-transporter 2 inhibitor, as a second-line treatment for non-alcoholic fatty liver disease patients with type 2 diabetes mellitus who do not respond to incretin-based therapies including glucagon-like peptide-1 analogs and dipeptidyl peptidase-4 inhibitors. *Clin Drug Investig*. 2016;36(4):313–319.
5. Ferrannini E, et al. Metabolic response to sodium-glucose cotransporter 2 inhibition in type 2 diabetic patients. *J Clin Invest*. 2014;124(2):499–508.
6. Merovci A, et al. Dapagliflozin improves muscle insulin sensitivity but enhances endogenous glucose production. *J Clin Invest*. 2014;124(2):509–514.

7. Daniele G, et al. Dapagliflozin enhances fat oxidation and ketone production in patients with type 2 diabetes. *Diabetes Care*. 2016;39(11):2036–2041.
8. Ferrannini E, et al. Shift to fatty substrate utilization in response to sodium-glucose cotransporter 2 inhibition in subjects without diabetes and patients with type 2 diabetes. *Diabetes*. 2016;65(5):1190–1195.
9. Fralick M, Schneeweiss S, Patorno E. Risk of diabetic ketoacidosis after initiation of an SGLT2 inhibitor. *N Engl J Med*. 2017;376(23):2300–2302.
10. Rosenstock J, Ferrannini E. Euglycemic diabetic ketoacidosis: a predictable, detectable, and preventable safety concern with SGLT2 inhibitors. *Diabetes Care*. 2015;38(9):1638–1642.
11. Ferrannini G, Hach T, Crowe S, Sanghvi A, Hall KD, Ferrannini E. Energy balance after sodium-glucose cotransporter 2 inhibition. *Diabetes Care*. 2015;38(9):1730–1735.
12. Hohendorff J, et al. A single dose of dapagliflozin, an SGLT-2 inhibitor, induces higher glycosuria in GCK- and HNF1A-MODY than in type 2 diabetes mellitus. *Endocrine*. 2017;57(2):272–279.
13. Long JZ, et al. The secreted enzyme PM20D1 regulates lipidated amino acid uncouplers of mitochondria. *Cell*. 2016;166(2):424–435.
14. Roberts LD, et al. β-Aminoisobutyric acid induces browning of white fat and hepatic β-oxidation and is inversely correlated with cardiometabolic risk factors. *Cell Metab*. 2014;19(1):96–108.
15. Hawley SA, et al. The Na+/glucose cotransporter inhibitor canagliflozin activates AMPK by inhibiting mitochondrial function and increasing cellular AMP levels. *Diabetes*. 2016;65(9):2784–2794.
16. Badman MK, Pissios P, Kennedy AR, Koukos G, Flier JS, Maratos-Flier E. Hepatic fibroblast growth factor 21 is regulated by PPARalpha and is a key mediator of hepatic lipid metabolism in ketotic states. *Cell Metab*. 2007;5(6):426–437.
17. Owen BM, et al. FGF21 acts centrally to induce sympathetic nerve activity, energy expenditure, and weight loss. *Cell Metab*. 2014;20(4):670–677.
18. Douris N, et al. Central fibroblast growth factor 21 browns white fat via sympathetic action in male mice. *Endocrinology*. 2015;156(7):2470–2481.
19. Douris N, et al. Beta-adrenergic receptors are critical for weight loss but not for other metabolic adaptations to the consumption of a ketogenic diet in male mice. *Mol Metab*. 2017;6(8):854–862.
20. Shin AC, et al. Brain insulin lowers circulating BCAA levels by inducing hepatic BCAA catabolism. *Cell Metab*. 2014;20(5):898–909.
21. Maida A, et al. Repletion of branched chain amino acids reverses mTORC1 signaling but not improved metabolism during dietary protein dilution. *Mol Metab*. 2017;6(8):873–881.
22. Nogiec C, Burkart A, Dreyfuss JM, Lerin C, Kasif S, Patti ME. Metabolic modeling of muscle metabolism identifies key reactions linked to insulin resistance phenotypes. *Mol Metab*. 2015;4(3):151–163.
23. Rhee EP, et al. Lipid profiling identifies a triacylglycerol signature of insulin resistance and improves diabetes prediction in humans. *J Clin Invest*. 2011;121(4):1402–1411.
24. Samuel VT, Petersen KF, Shulman GI. Lipid-induced insulin resistance: unravelling the mechanism. *Lancet*. 2010;375(9733):2267–2277.
25. Hardivillé S, Hart GW. Nutrient regulation of signaling, transcription, and cell physiology by O-GlcNAcylation. *Cell Metab*. 2014;20(2):208–213.
26. Iroz A, et al. A specific ChREBP and PPARα cross-talk is required for the glucose-mediated FGF21 response. *Cell Rep*. 2017;21(2):403–416.
27. Jois T, et al. Deletion of hepatic carbohydrate response element binding protein (ChREBP) impairs glucose homeostasis and hepatic insulin sensitivity in mice. *Mol Metab*. 2017;6(11):1381–1394.
28. Bonner C, et al. Inhibition of the glucose transporter SGLT2 with dapagliflozin in pancreatic alpha cells triggers glucagon secretion. *Nat Med*. 2015;21(5):512–517.
29. Wang MY, et al. Dapagliflozin suppresses glucagon signaling in rodent models of diabetes. *Proc Natl Acad Sci USA*. 2017;114(25):6611–6616.
30. Xu L, et al. SGLT2 inhibition by empagliflozin promotes fat utilization and browning and attenuates inflammation and insulin resistance by polarizing M2 macrophages in diet-induced obese mice. *EBioMedicine*. 2017;20:137–149.
31. Inagaki T, et al. Endocrine regulation of the fasting response by PPARalpha-mediated induction of fibroblast growth factor 21. *Cell Metab*. 2007;5(6):415–425.
32. Badman MK, Koester A, Flier JS, Kharitonenkov A, Maratos-Flier E. Fibroblast growth factor 21-deficient mice demonstrate impaired adaptation to ketosis. *Endocrinology*. 2009;150(11):4931–4940.
33. Bookout AL, et al. FGF21 regulates metabolism and circadian behavior by acting on the nervous system. *Nat Med*. 2013;19(9):1147–1152.
34. Coskun T, et al. Fibroblast growth factor 21 corrects obesity in mice. *Endocrinology*. 2008;149(12):6018–6027.
35. Ding X, et al. βKlotho is required for fibroblast growth factor 21 effects on growth and metabolism. *Cell Metab*. 2012;16(3):387–393.
36. Huang Z, et al. The FGF21-CCL11 axis mediates beiging of white adipose tissues by coupling sympathetic nervous system to type 2 immunity. *Cell Metab*. 2017;26(3):493–508.e4.
37. Fisher FM, et al. FGF21 regulates PGC-1α and browning of white adipose tissues in adaptive thermogenesis. *Genes Dev*. 2012;26(3):271–281.
38. Robles-Valdes C, McGarry JD, Foster DW. Maternal-fetal carnitine relationship and neonatal ketosis in the rat. *J Biol Chem*. 1976;251(19):6007–6012.
39. Izumida Y, et al. Glycogen shortage during fasting triggers liver-brain-adipose neurocircuitry to facilitate fat utilization. *Nat Commun*. 2013;4:2316.
40. Sengupta S, Peterson TR, Laplante M, Oh S, Sabatini DM. mTORC1 controls fasting-induced ketogenesis and its modulation by ageing. *Nature*. 2010;468(7327):1100–1104.
41. Hirschey MD, et al. SIRT3 regulates mitochondrial fatty-acid oxidation by reversible enzyme deacetylation. *Nature*. 2010;464(7285):121–125.
42. von Meyenn F, et al. Glucagon-induced acetylation of Foxa2 regulates hepatic lipid metabolism. *Cell Metab*. 2013;17(3):436–447.

43. Gut P, Verdin E. The nexus of chromatin regulation and intermediary metabolism. *Nature*. 2013;502(7472):489–498.
44. Chau MD, Gao J, Yang Q, Wu Z, Gromada J. Fibroblast growth factor 21 regulates energy metabolism by activating the AMPK-SIRT1-PGC-1alpha pathway. *Proc Natl Acad Sci USA*. 2010;107(28):12553–12558.
45. Jin W, et al. Increased SRF transcriptional activity in human and mouse skeletal muscle is a signature of insulin resistance. *J Clin Invest*. 2011;121(3):918–929.
46. Roberts LD, Souza AL, Gerszten RE, Clish CB. Targeted metabolomics. *Curr Protoc Mol Biol*. 2012;98(1):30.2.1–30.2.24.
47. Leek JT, et al. Tackling the widespread and critical impact of batch effects in high-throughput data. *Nat Rev Genet*. 2010;11(10):733–739.
48. Ritchie ME, et al. Empirical array quality weights in the analysis of microarray data. *BMC Bioinformatics*. 2006;7:261.
49. Ritchie ME, et al. limma powers differential expression analyses for RNA-sequencing and microarray studies. *Nucleic Acids Res*. 2015;43(7):e47.
50. Wu D, Lim E, Vaillant F, Asselin-Labat ML, Visvader JE, Smyth GK. ROAST: rotation gene set tests for complex microarray experiments. *Bioinformatics*. 2010;26(17):2176–2182.
51. Fabregat A, et al. The reactome pathway knowledgebase. *Nucleic Acids Res*. 2018;46(D1):D649–D655.